Photodetachment spectrum of OHF^-: Three-dimensional study of the heavy–light–heavy resonances

Lola González-Sánchez
Unidad Asociada UAM-CSIC, Instituto de Matemáticas y Física Fundamental, C.S.I.C., Serrano 123, 28006 Madrid, Spain and Departamento de Química Física, Facultad de Química, Universidad de Salamanca, 37008 Salamanca, Spain

Susana Gómez-Carrasco
Departamento de Física de la Atmósfera, Facultad de Ciencias and Departamento de Química Física, Facultad de Química, Universidad de Salamanca, 37008 Salamanca, Spain and Unidad Asociada UAM-CSIC, Departamento de Química Física, Facultad de Ciencias C-XIV, Universidad Autónoma de Madrid, 28049 Madrid, Spain

Alfredo Aguado and Miguel Paniagua
Unidad Asociada UAM-CSIC, Departamento de Química Física, Facultad de Ciencias C-XIV, Universidad Autónoma de Madrid, 28049 Madrid, Spain

M. Luz Hernández and José M. Alvariño
Departamento de Física de la Atmósfera, Facultad de Ciencias and Departamento de Química Física, Facultad de Química, Universidad de Salamanca, 37008 Salamanca, Spain

Octavio Roncero
Unidad Asociada UAM-CSIC, Instituto de Matemáticas y Física Fundamental, C.S.I.C., Serrano 123, 28006 Madrid, Spain

(Received 17 February 2004; accepted 7 April 2004)

In this work a simulation of the OHF^- photodetachment spectrum is performed in a three-dimensional potential energy surface recently developed for $OHF(^3A'')$. The ground $^2A'$ state potential of the anion is calculated in three dimensions based on accurate *ab initio* calculations and the reaction dynamics is studied using a wave packet method. The calculated spectrum shows a sequence of bands associated to vibrational $HF(v)$ up to $v=3$. Each band is formed by a continuous spectrum and resonant structures. These resonances are associated to the OH–F channel well of the $^3A''$ PES, in which fragmentation occurs through vibrational predissociation. Above the $OH(v=0)$ threshold a new resonant pattern appears corresponding to heavy–light–heavy resonances. Special attention is paid to the assignment of these resonances because they mediate the reaction dynamics in the OH+F collision at low kinetic energies. The sequence of bands is in rather good agreement with that appearing in the experimental spectrum, especially at higher electron kinetic energies. At low kinetic energies, however, some other electronic states may contribute. The resonance structures might be washed out by the rotational average and the relatively low energy resolution of the experiment. © *2004 American Institute of Physics.* [DOI: 10.1063/1.1756581]

I. INTRODUCTION

The importance of the catalytic ozone destruction cycle by halogen atoms gives a great interest to the $O(^3P)+HX$ reactions, since the hydrogen halides constitute the dominant ''temporary sink'' of atomic halogens.[1] The most important among them, because of its abundance in the atmosphere, is chlorine, widely studied both experimentally[2–7] and theoretically.[2,8–16] Such reactions present the difficulty of dealing with open shell systems, which involves the necessity of using several coupled electronic states to properly simulate the reaction dynamics. The study of nonadiabatic processes requires in turn a very large effort in the modelization of several coupled potential energy surfaces (PES). For this reason, the lighter member of this family, HF+O, may be considered as a benchmark system in which more accurate *ab initio* calculations and detailed quantum dynamical simulations can be performed.

In contrast to the analogous HCl+O reaction, which is nearly thermoneutral, the $HF+O(^3P)\rightarrow OH+F$ reaction is very endoergic, by approximately 1.5 eV. The reverse OH+F reaction involves two radical species, what is an inherent experimental problem. So, until now only few experimental kinetic (but, unfortunately, no beam experiments) studies on the temperature effect on the rate constants[17] and infrared chemiluminiscence spectra for final vibrational states of HF products[18] are available under multiple collisions conditions. Recently, we have studied theoretically the OH+F reactive collisions[19,20] on a new global PES of the ground $^3A''$ electronic state.[20] This new PES is based on very accurate *ab initio* calculations described in detail in Ref. 20 (hereafter called paper I). This PES, in contrast to previous results,[18] does not show a real barrier to reaction. The final HF vibrational distributions obtained in the new PES[19,20] are in rather good agreement with the available experimental results of

Sloan and co-workers.[18] They suggested a transition between a triplet and a singlet state, because their PES predicted a barrier too high to allow the reaction on triplet ground state. But, with the new $^3A''$ PES, the reaction can take place on it without necessarily invoking any intersystem crossing.

The $OH(v=0)+F$ reaction presents a dynamical barrier, essentially due to the zero-point energy for the vibrational modes near the saddle point.[20] Above this threshold the reaction is direct, presenting an important constraint because of the small skew angle associated to all heavy–light–heavy (HLH) systems: the reaction presents important vector correlation,[20] being favored when OH rotational angular momentum, **j**, is perpendicular to the initial relative velocity vector between the two reagents, **k**. Below the dynamical threshold the reaction is mediated by resonances occurring near the transition state region. Such HLH resonance structures also appear in quasiclassical simulations of the reactive collisions,[20] which must be associated to periodic orbits on the top of the saddle point.

The photoelectron detachment spectroscopy experiment performed by Neumark and co-workers[21] on this system presents a particularly interesting alternative to the detailed study of such resonances. At this regard, all the previous theoretical simulations[21,22] have been restricted to collinear OHF geometries, the equilibrium geometry of OHF^-. First, Neumark and co-workers calculated the $^2\Pi$ and $^2\Sigma$ electronic states of OHF^- and simulated the spectrum using the collinear PES's obtained by Sloan *et al.*[18] for the neutral OHF system. The fact of considering a too high reaction barrier was later corrected by Dixon and Tachikawa.[22] They reported better *ab initio* calculations of the anionic and neutral species, but they only considered simulations of the spectrum at collinear configuration.

The aim of this work is the study of the photodetachment spectrum on the ground $^3A''$ state, using the three-dimensional global PES recently reported by us.[19,20] The structure of the spectrum will be discussed and assigned, paying special attention to the heavy–light–heavy (HLH) resonances appearing above the OH+F rearrangement channel. This kind of resonance typically appears when two different rearrangement channels, HL+H′ and H+LH′, are open. In such situation, the light hydrogen atom oscillates between the two heavy atoms, providing important information on the transition state region, as widely studied by Neumark and co-workers.[23,24] Typically, most of the systems studied are either symmetric, like XHX[25,26] (with X being an halogen atom) or nearly thermoneutral as OHCl.[7,9] Meanwhile, the OH+F reaction is very exothermic, and allows the gradual study about the opening of the second rearrangement channel and its effect on the HLH′ resonances. At low energies as $OH(v=0)$ is closed, the HF vibrations will be well separated from the O–HF vibrations, whose frequency is determined by the shallow well in the products valley. At higher energies, just below the $OH(v=0)$ threshold, the OH and HF vibrations have similar frequencies and important intramolecular vibrational redistribution (IVR) must distort the spectrum, because the OH+F channel can be explored. Finally, when the $OH(v=0)$ channel opens up the competition between the dissociation through the two rearrangement channels could be analyzed.

II. THE OHF^- PRECURSOR

A. *Ab initio* electronic structure calculations

Details of the *ab initio* calculations performed for the neutral OHF system have been given in paper I. For OHF^- a more polarizable basis set is needed. For that purpose, the aug-cc-pVTZ basis set of contracted Gaussians functions of Dunning and co-workers[27,28] used in the neutral OHF system was augmented by the addition of extra diffuse functions to reproduce the Rydberg states of atomic hydrogen. The molecular orbitals were optimized in a complete active space (CASSCF) procedure.[29] These CASSCF wave functions were used as reference in subsequent internally contracted multireference configuration interaction (MRCI) calculations,[30,31] with single and double excitations, including all the valence electrons for the correlation. The Davidson extrapolation size consistency correction[32] was used. All the calculations were carried out using the MOLPRO suite of *ab initio* programs,[33] using the C_s group to avoid discontinuities near the collinear configuration.

The goal of these calculations is only to reproduce the well of the OHF^- anion to calculate the first bound states needed as initial states to study the photon excitation. A deeper description on the structure and dissociation energies can be found elsewhere.[21] For all the nuclear configurations considered, the electronic energy of the anion is lower than that for the neutral. At collinear configurations, the ground state is $^2\Pi$, while the first excited $^2\Sigma$ state is relatively higher in energy, as shown in Fig. 1, in agreement with previous calculations.[21,22] As the system bends, the two $^2\Pi$ states split, see Fig. 1(c) being that of $^2A'$ symmetry the ground state. In this work, we shall restrict our attention to the ground $^2A'$ electronic state.

More than 1800 points were computed in the vicinity of the minimum of the OHF^- well, located at collinear O–H–F configuration with $R_{OH}\approx 1.08$ and $R_{HF}\approx 1.32$ Å, in good agreement with values obtained by Bradforth *et al.*,[21] $R_{OH}\approx 1.08$ and $R_{HF}\approx 1.35$ Å. The *ab initio* calculations were performed for O–H–F angles equal to 180°, 170°, 165°, and 150° considering 15 points for the R_{FO} distance in the interval [1.59, 3.44] Å and 31 points for R_{HF} variable in the interval [0.53, 2.12] Å.

An analytical local fit of the PES in the region of the minimum was done using the method developed by Aguado and Paniagua.[34] (This fit can be obtained upon request.) Two cuts of the PES are presented in Fig. 2 in Jacobi coordinates, with **r** being the HF internuclear vector, **R** the vector joining the HF center of mass to the O atom, and γ the angle between the two vectors. These coordinates, hereafter used for the dynamics, are called ''product'' coordinates in consideration to the OH+F→HF+O reactive collisions studied in paper I, in which OH–F ''reactant'' Jacobi coordinates were used.

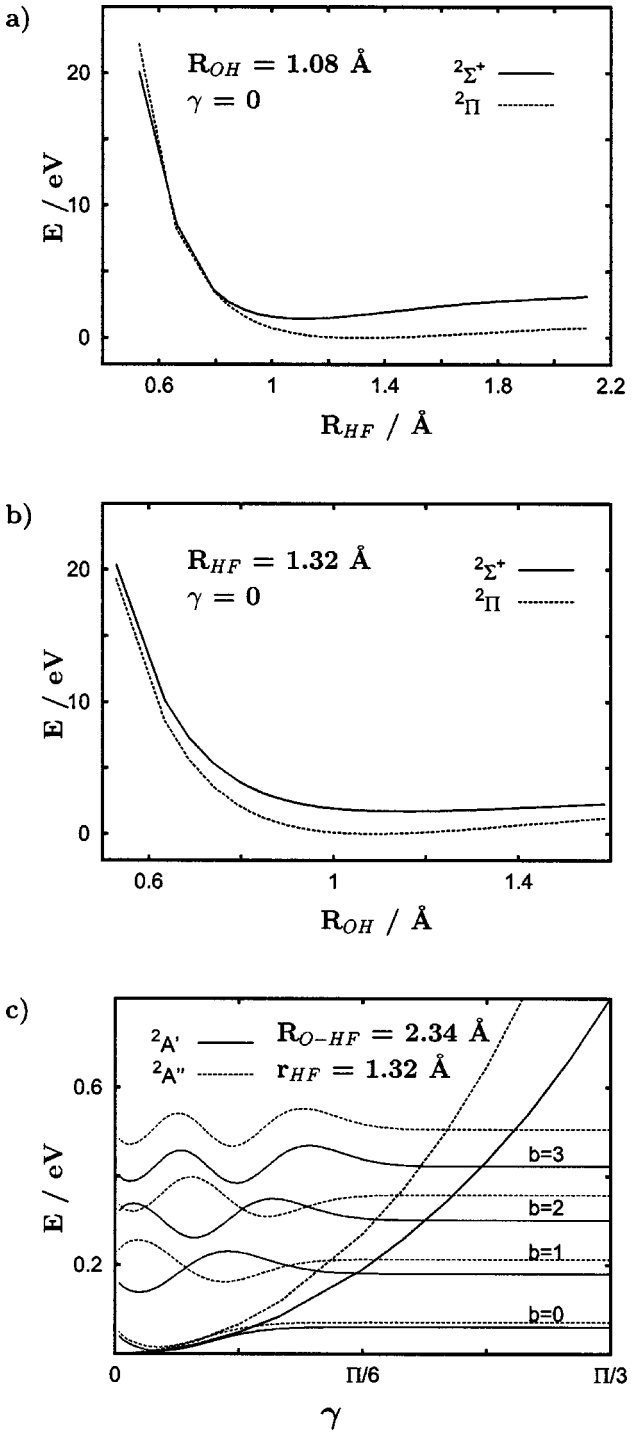

FIG. 1. Calculated *ab initio* energy points for several electronic states of the OHF^- anion. On each panel fixed geometric parameters are equilibrium values. On panel (c) the two potential curves, of $^2A'$ (solid line) and $^2A''$ (dashed line) states, are plotted together with their corresponding monodimensional bending levels, *b*.

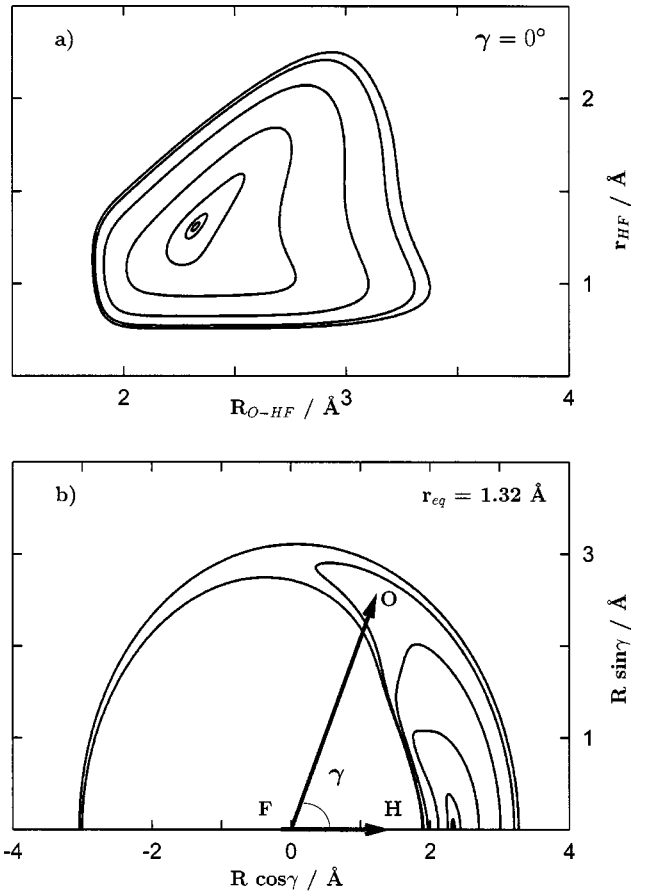

FIG. 2. Contour plots of the local $OHF^-(^2A')$ PES in product Jacobi coordinates for (a) $\gamma=0$, (b) $r=1.32$ Å, with $x=R\cos\gamma$ and $y=R\sin\gamma$. The contours correspond to 0.002, 0.01, 0.1, 1, 5, 10, and 12 eV.

B. Bound states

In the Born–Oppenheimer approximation, the total wave function of the initial bound state of OHF^- is written as the product of a bound electronic function, χ_α^- (where the superscript minus is introduced to distinguish the OHF^- anion from the neutral OHF, and α labels the electronic states), times the nuclear function, $\Phi_k^{JMp\alpha}$, where k refers to the vibrational state, and J,M are the total angular momentum and its projection. The corresponding eigenvalue is $E_{\alpha,k}^-$.

Using product Jacobi coordinates in a body-fixed frame, in which the three atoms lie on the $x-z$ plane, with the z axis being parallel to the **R** Jacobi vector, the $\Phi_k^{JMp\alpha}$ bound states are expanded as

$$\Phi_k^{JMp\alpha}(\mathbf{r},\mathbf{R})=\sum_{vsj\Omega} A_{vsj\Omega}^{Jp\alpha k}\frac{\varphi_v(r)}{r}\frac{\phi_s(R)}{R}\mathcal{W}_{M\Omega}^{Jp}Y_{j\Omega}(\gamma,0), \tag{1}$$

where the angular functions, defined as

$$\mathcal{W}_{M\Omega}^{Jp}=\sqrt{\frac{2J+1}{16\pi^2(1+\delta_{\Omega 0})}}[D_{M,\Omega}^{J*}(\phi,\theta,\chi) + p(-1)^{J+\Omega}D_{M,-\Omega}^{J*}(\phi,\theta,\chi)],$$

correspond to a well defined J and p, the parity under inversion of spatial coordinates. M and Ω are the projections of the total angular momentum in the space-fixed and body-fixed z axes, respectively. $D_{M,\Omega}^{J*}$ are Wigner rotation matrices and $Y_{j,\Omega}$ are normalized associated Legendre functions.[35] The $\varphi_v(r)$ and $\phi_s(R)$ radial functions are numerical solutions of a Hamiltonian with monodimensional potentials specially optimized to reproduce the PES at equilibrium. Details of the calculations can be found elsewhere.[36]

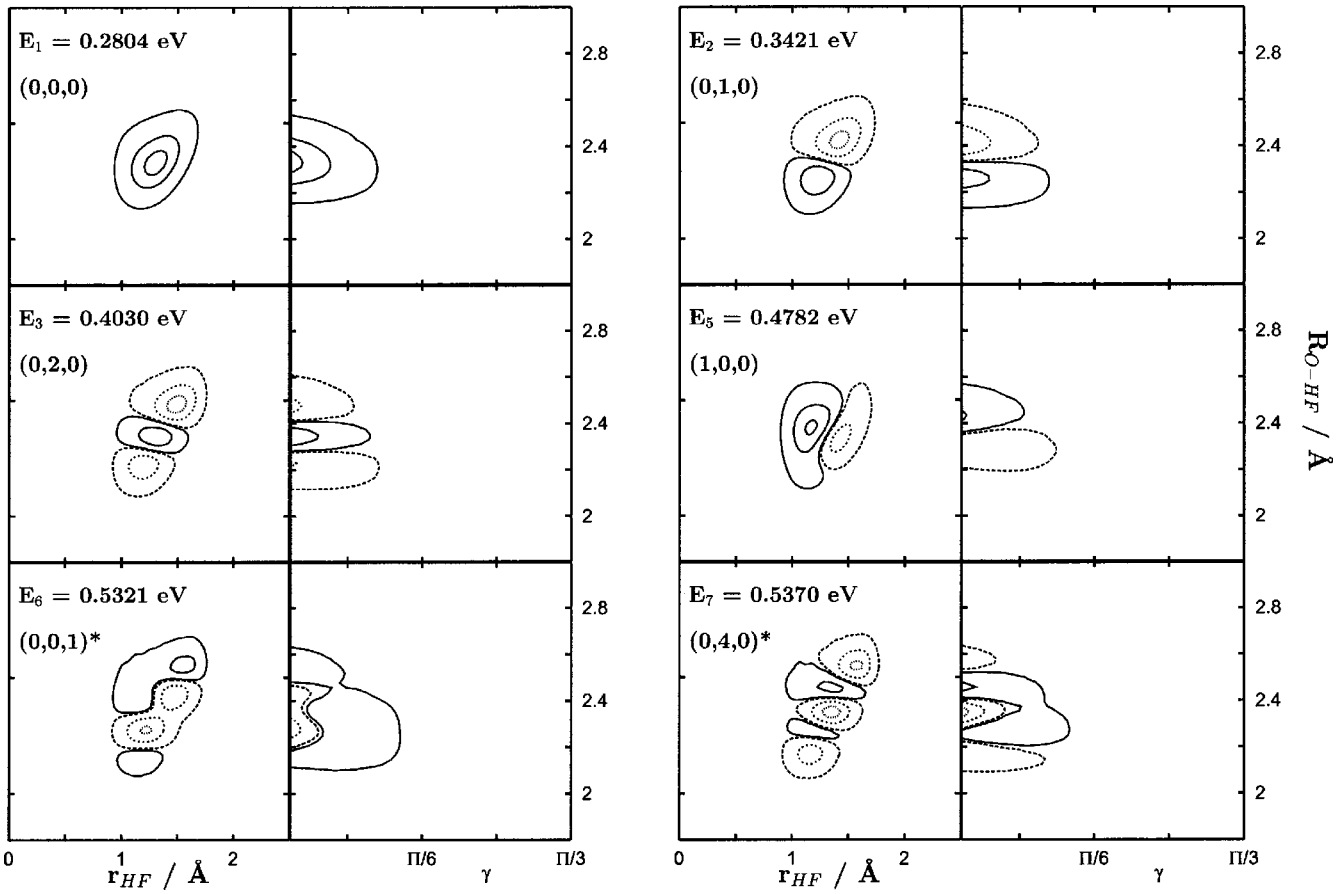

FIG. 3. Contour plots of the wave function amplitude for several vibrational bound states of $OHF^-(^2A')$ in product Jacobi coordinates for $\gamma=0$ (left panels) and for $r=1.32$ Å (right panels). The energies, E_k of the k level are in eV, and the approximate (v,n,b) quantum numbers are given. Solid (dashed) lines correspond to positive (negative) amplitudes. The levels marked with an asterisk interact strongly.

In Fig. 3, contour plots of the lower bound states are shown for total angular momentum $J=0$, with their energies. The approximate quantum numbers used to label those vibrational states correspond to the three internal motions associated to product Jacobi coordinates: v, the HF vibrational quantum number, n the quantum number for the vibration of O atom with respect to the HF center-of-mass, and b the quantum number for the bending motion, characterized by the angle γ between the two Jacobi vectors. In a linear molecule, there are two components of the bending vibration, one for the A' symmetry, considered in this ground state, and a second of A'' symmetry in the first excited state. The frequencies associated to the ground A' state are $\omega_R \approx 62$ meV very much different from the other two, $\omega_r \approx 0.2$ eV and $\omega_\gamma \approx 0.25$ eV. For the first excited A'' state of the anion it can be considered at zero order that ω_R and ω_r are approximately equal to those of the A' state. Using a monodimensional angular solution, in Fig. 1(c), the ground level in the $^2A''$ state is ≈ 19 meV above the ground level of the $^2A'$ state. Even these 19 meV are relatively large as compared to the low temperatures of the OHF^- precursor in the experiments, ≈ 10 K. Averaging over rotational states seems to play a more important role in the more precise simulation of the photodetachment experiment. However, only one single rotational transition from the ground vibrational level will be considered here to analyze the details of the spectrum. The spectra from different vibrational initial states of the anion have been described by Dixon and Tachikawa[22] in a collinear model.

III. SPECTRA CALCULATIONS ON THE GROUND ELECTRONIC STATE

A. Three-dimensional wave-packet calculations

A complete treatment of photodetachment spectra can be found elsewhere,[37] and here a brief outline of the most important approximations is discussed. The photoexcited system dissociates in three fragments, the electron and two neutral molecular products. The total absorption cross section from a single initial state of the anion may be expressed as

$$\sigma(h\nu) = \int d\epsilon\, \sigma(h\nu, \epsilon), \tag{2}$$

where ϵ is the kinetic energy of the ejected electron while $h\nu$ is the energy of the incident photon, and $\sigma(h\nu,\epsilon)$ is the measured partial cross section as a function of the electron kinetic energy. The energy remaining for the neutral system is thus $E = E^-_{\alpha,k} + h\nu - \epsilon$.

Assuming a first order perturbative treatment for an electric dipole transition, and the Born–Oppenheimer approximation for the excited system, the partial cross section is expressed as

$$\sigma(h\nu,\epsilon)\propto\sum_{\Gamma,\beta}|\langle\Phi_k^{JMp\alpha}\chi_\alpha^-|\mathbf{d}\cdot\mathbf{e}|\Phi_{\Gamma,\beta,E}^{J'M'p'\alpha'\epsilon}\chi_{\alpha',\epsilon}\rangle|^2, \quad (3)$$

where $\chi_{\alpha',\epsilon}$ is the electronic wave function corresponding asymptotically to the α' electronic state of OHF plus the ejected electron with kinetic energy ϵ. $\Phi_{\Gamma,\beta,E}^{J'M'p'\alpha'\epsilon}$ is the dissociative nuclear part of the wave function corresponding asymptotically to a particular rovibrational state, β, of the nuclear fragments of the Γ rearrangement channel. Finally, **e** is the electric polarization vector of the incident light and **d** is the electric dipole moment of the molecular system.

Since the ejection of the electron is very fast, the electronic wave function may be factorized as the simple product of an *s*-wave function of the ejected electron times that of the remaining OHF system, $\chi_{\alpha',\epsilon}\approx\chi_\epsilon\chi_{\alpha'}$. The nuclear wave function is considered to be independent of the ejected electron, $\Phi_{\Gamma,\beta,E}^{J'M'p'\alpha'\epsilon}\approx\Phi_{\Gamma,\beta,E}^{J'M'p'\alpha'}$, so that the partial cross section of Eq. (3) can be expressed similarly to that of a simpler photodissociation process as

$$\sigma(h\nu,\epsilon)\approx\sigma(E)\propto\sum_{\Gamma,\beta}|\langle\Phi_k^{JMp\alpha}|\mathbf{d}^{\alpha,\alpha'\epsilon}\cdot\mathbf{e}|\Phi_{\Gamma,\beta,E}^{J'M'p'\alpha'}\rangle|^2, \quad (4)$$

except for the dependence of the transition dipole moments on the ejected electron, given by $\mathbf{d}^{\alpha,\alpha'\epsilon}=\langle\chi_\alpha^-|\mathbf{d}|\chi_\epsilon\chi_{\alpha'}\rangle$. These moments, however, can also be considered to be independent on the kinetic energy of the ejected electron, i.e., $\mathbf{d}^{\alpha,\alpha'\epsilon}\approx\mathbf{d}^{\alpha,\alpha'}$. In this situation, Eq. (4) becomes completely equivalent to that of the spectrum for normal photodissociation, since all the dependence on the ejected electron has been eliminated because its dynamics is much faster.

Moreover, since the initial vibrational bound state is localized in a rather small region, the transition dipole moments can be also considered to be constant as a function of the internal degrees of freedom. For the three-dimensional model presented in this section only the $^3A''$ state of OHF will be considered, which correlates either to a $^3\Pi$ or a $^3\Sigma^-$ state, depending on the geometry. Because for collinear configuration the electronic state of the anion is $^2\Pi$, there will be contributions from parallel as well as perpendicular transitions. Here it will be assumed that the transition is isotropically distributed in the *xz* body-fixed frame.

In order to calculate the partial cross section, in Eq. (4), a wave packet method is used in which

$$\sigma(E)=\frac{1}{\pi\hbar}\mathcal{R}\int_0^\infty dt\, e^{iEt/\hbar}\ \langle\Psi(t=0)|\Psi(t)\rangle, \quad (5)$$

with the initial wave packet defined as[38,39]

$$\Psi(t=0)=\sum_{\Omega'}\mathcal{W}_{M',\Omega'}^{J'p'}\langle\mathcal{W}_{M',\Omega'}^{J'p'}|\mathbf{d}^{\alpha'\alpha}\cdot\mathbf{e}|\Psi_k^{JMp\alpha}\rangle. \quad (6)$$

The propagation of the wave packet is performed using the global three-dimensional PES of Paper I[20] using a Chebyshev propagator[40,41] in which the wave packet is multiplied by an absorbing damping function after each time step, as previously described.[38,39] The parameters used in the propagation are summarized in Table I.

TABLE I. The wave packet is absorbed at each time step by multiplying the wave packet by $f_1(r)f_2(R)$, where $f_i(x)=\exp[-\alpha_{\text{abs}}(x-x_{\text{abs}})^2]$.

No. angles	100	
$\Delta\mathbf{t}$	1 fs	
$\mathbf{t}_{\text{final}}$	4 ps	
	$\mathbf{r}_{\text{HF}}$	$\mathbf{R}_{\text{O–HF}}$
No. points	160	384
$\mathbf{r}_{\text{ini}}$/Å	0.4	0.5
$\mathbf{r}_{\text{fin}}$/Å	9.0	15.0
α_{abs}/Å^{-2}	0.5	0.5
$\mathbf{x}_{\text{abs}}$/Å	6.0	10.0

The initial wave packet built to simulate the $J'=1\leftarrow J=0$ rotational transition, in Fig. 4, lies on the transition state region. As time evolves, most of the density departs rather rapidly, mainly in the HF+O channel. An important part of the wave packet remains ''trapped'' in the region of the well of $\approx$0.25 eV depth in the HF+O channel, as a clear manifestation of resonances. Such relatively deep well is due to a sort of hydrogen bond which strongly stabilize the OH–F and FH–O complexes.[20] The calculated partial cross section is presented in Fig. 5. As in the cases previously reported,[21,22] the spectrum is formed by several bands, which were attributed to different vibrational states of the HF fragments. A crucial feature in our results is the presence of narrow resonances, which were not present in the previous modelizations.[21,22] The experimental spectrum does not show narrow resonances, but they may be washed out by rotational average or by the low energy resolution. In particular, the two peaks just below and above $\epsilon\approx0.5$ eV in the experimental spectrum (labeled E and F) are placed near the two groups of calculated resonances. These structures appear at high OHF energies and will be shown to be due to the absorption to several final electronic states,[42] and not only to the $^3A''$ state studied here. At low energies however, this last state plays a major role because only two other triplet states may contribute, with similar minimum energy paths. The absorption to the $^3A''$ state presents a sequence of bands whose energy separation is in pretty good agreement with the experimental ones.

B. Assignment of bands

In order to check the previous assignments of the bands as associated to the vibrational levels of HF,[21,22] two different kinds of calculations have been done. First, the initial wave packet is projected into the different vibrational states of the HF products. Second, the final vibrational state distribution of the HF is calculated.

The first method consists in applying approximated projection operators to the initial wave packet to divide it into several portions.[43] The projection operators used are defined as

$$P=\sum_{v=0}^{2}P_v, \quad Q=1-P, \quad (7)$$

with

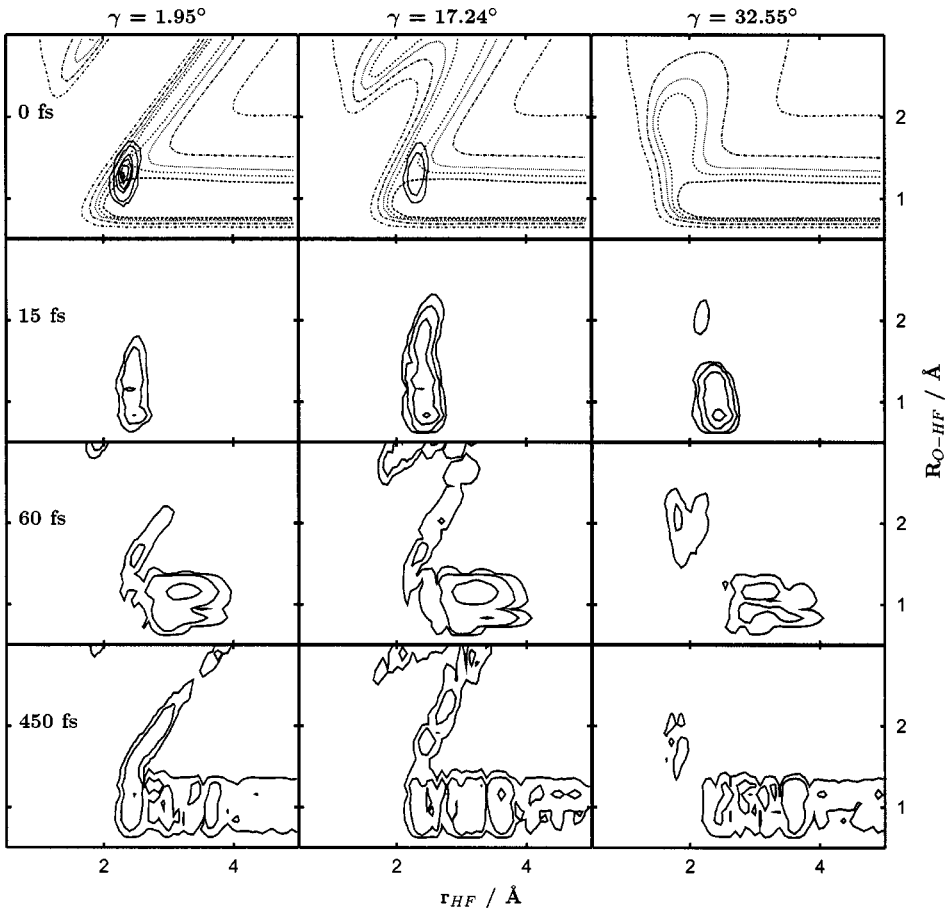

FIG. 4. Contour plots of the wave packet density for different times and angles in the product Jacobi coordinates. The propagation is performed on the OHF($^3A''$) PES to simulate the $J'=1\leftarrow J=0$. The contours of the potential correspond to 3.5, 1.5, 0.5, 0, -0.5 eV with respect to OH($v=0$) + F.

$$P_v=\sum_j \sum_\Omega |F_{vj\Omega}\rangle\langle F_{vj\Omega}| \tag{8}$$

and

$$F_{vj\Omega}=\frac{\varphi_{vj}(r)}{r} Y_{j\Omega}(\gamma,0) W^{J\epsilon}_{M\Omega}(\phi,\theta,\chi). \tag{9}$$

In this case, we have performed independent calculations for P_v, $v=0$, 1, and 2 and Q. If the spectrum is built independently for each propagation some interference terms are lost. Therefore, the procedure is approximated, unless the different portions of the wave packet correspond to different energy windows of the spectrum. In Fig. 6, the independent spectra for each of the portion of the initial wave packet thus obtained are shown. The sum of all of them gives qualitatively the total spectrum shown in Fig. 5, but not exactly. However, it serves to determine the origin of each band of the spectrum, corroborating the previous assignments.[21,22] To clarify this vibrational pattern, the energetics of the problem is shown in the minimum energy path, in Fig. 7.

In second place, the analysis of the final vibrational state distribution obtained using the method of Balint-Kurti *et al.*[44] (see also Ref. 38) in the propagation of the full wave packet is shown in Fig. 6. At low energy, there is always a dominant vibrational channel. The dissociation can be considered as a direct process, for the nearly continuous bands, or a vibrational predissociation, in the peaks associated to narrow resonances. In this regime, there is a clear connection between the initial vibrational state, responsible for the ab-

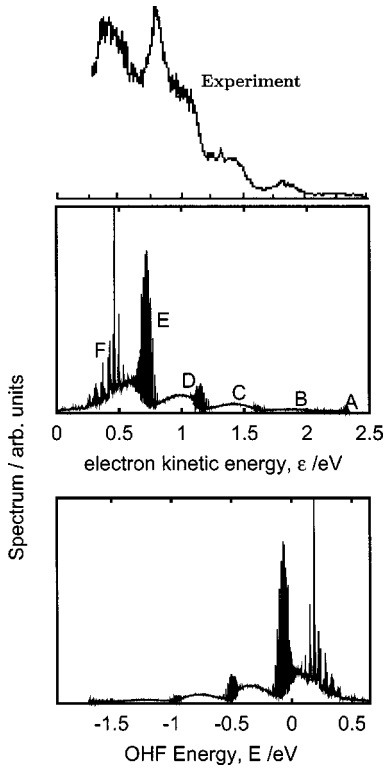

FIG. 5. Spectrum obtained for the $J'=1\leftarrow J=0$ transition. Bottom panel, as a function of the OHF energy. Central panel, as a function of the electron kinetic energy, using $\epsilon=0.65-E$ in eV. The factor 0.65 has been fitted, since the dissociation energy of the OHF^- was not calculated. Top panel, experimental spectrum from Ref. 21.

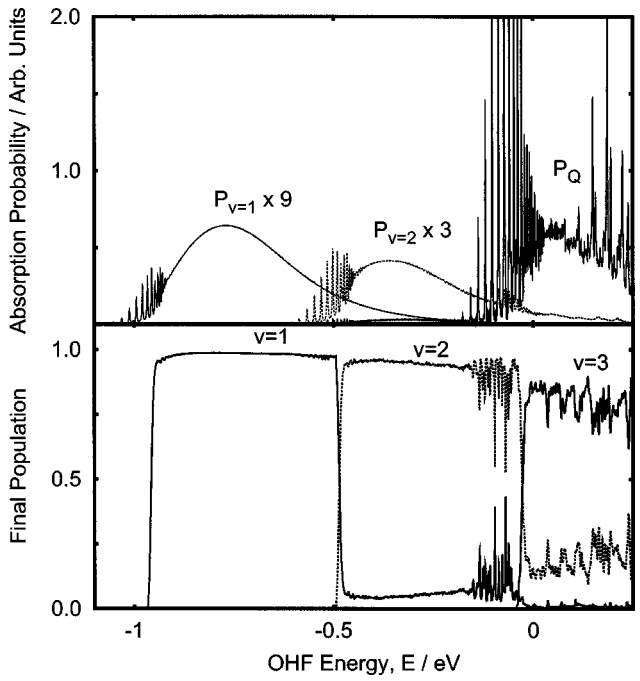

FIG. 6. Top panel, absorption probabilities obtained for the different portions of the wave packets applying the projection operators of Eq. (7). Bottom panel final HF(v) vibrational distribution. Energy scale, in eV, is referred to the F+OH($v=0$) threshold.

sorption, and the final vibrational state of HF, obtained after dissociation. The idea of assigning each band to a particular vibrational level of HF is thus corroborated. At high energies, however, the wave packet can also explore the OH+F channel, and there is the opportunity of IVR processes, so that the final vibrational distribution is much wider.[45] Whenever the OH($v=0$)+F channel is open (the zero of energy), the resonances become much broader and erratically distributed in energy. It is at these energies where the light H atom can be considered to be oscillating between the two heavier atoms, and the so-called HLH' resonances can be detected.

Therefore, it may be concluded that the bands can be associated definitely to the HF vibrational levels. To further analyze the structure of the spectrum, especially the features of the resonances as a function of internal energy, we shall present some simple models for clarification.

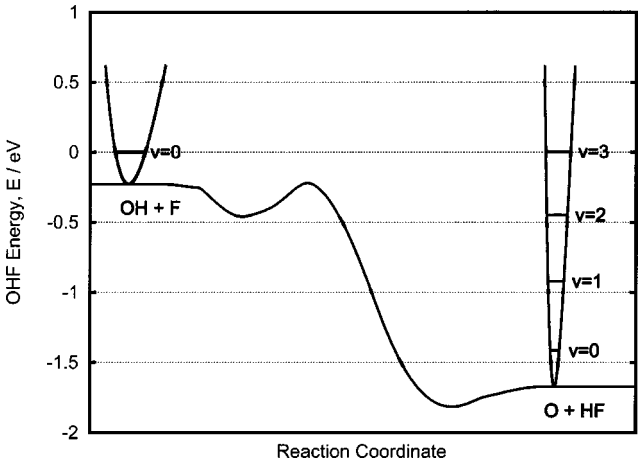

FIG. 7. Minimum energy path (in eV) describing the OH+F→HF+O in the $^3A''$ adiabatic energy surface. The vibrational levels of each of the asymptotes obtained with the present PES are also indicated.

C. Resonances below OH+F threshold

The HF equilibrium distance, r_e, in the OHF^- anion is larger than that of free HF, so that the maximum of the amplitude associated to the ground vibrational state coincides with HF($v\approx4$), see right panel of Fig. 8. As a consequence, the intensity of the bands should increase as v increases up to that of $v=4$ or 5. However, at $v=3$, the OH channel opens, see Fig. 7, what makes that the outer classical turning point disappears, thus explaining why the spectrum intensity decreases after the HF($v=3$) dissociation asymptote.

In contrast, the equilibrium R_e distance for OHF^- is considerably shorter than that of OHF at r_e. For neutral OHF, the collinear monodimensional potential, obtained averaging the PES with the free HF vibrational solutions, presents a well, as shown in Fig. 8. The overlap between the OHF^- radial function and the eigenstates of this monodimensional potential shows important Franck–Condon factors for excitation of the bound states supported by this well and also a very broad distribution corresponding to the direct excitation of the dissociative solution of each v channel. This explains the structure obtained for each vibrational channel.

When the coupling between the different vibrational channels is introduced, the bound states transform in resonances, whose width arises from a relatively slow vibrational predissociation (VP). The continuous distribution becomes even broader, so that the spectrum associated to each vibrational channel overlap with each other.

The well in the HF+O channel and that of OHF^- correspond to a collinear configuration. The Franck–Condon factors favor the overlap to those resonances corresponding to quasibound states with no bending excitation. The quasibound levels corresponding to $v=1$ are shown in Fig. 9, and have been obtained using the same procedure described in Sec. II B, but eliminating the $v=0$ functions of the basis set. Their energies are very good approximations to the position of the associated resonances that we can see in the panel of $v=1$ in Fig. 10, with a little displacement. The sequences of stretching and bending are different for lower energies, but for higher energies they are mixed.

It is difficult to converge the calculations below zero using wave packet methods. The presence of narrow resonances requires long propagation times while the broad energy range of the spectrum requires small time steps. For this purpose we have also performed time-independent close coupling (TICC) calculations using a reduced vibrational ($v=0-7$) and rotational ($j=0-40$) basis set of the HF fragments. With the method described elsewhere,[46,47] it is possible to resolve the resonant structure of the spectrum at low energies. Below zero, the discrepancies between the two calculations, in Fig. 10 are due to the lack of convergence of the wave packet calculations, and the TICC results are more accurate.

For energies above zero, however, the TICC method with the limited basis set cannot properly describe the OH

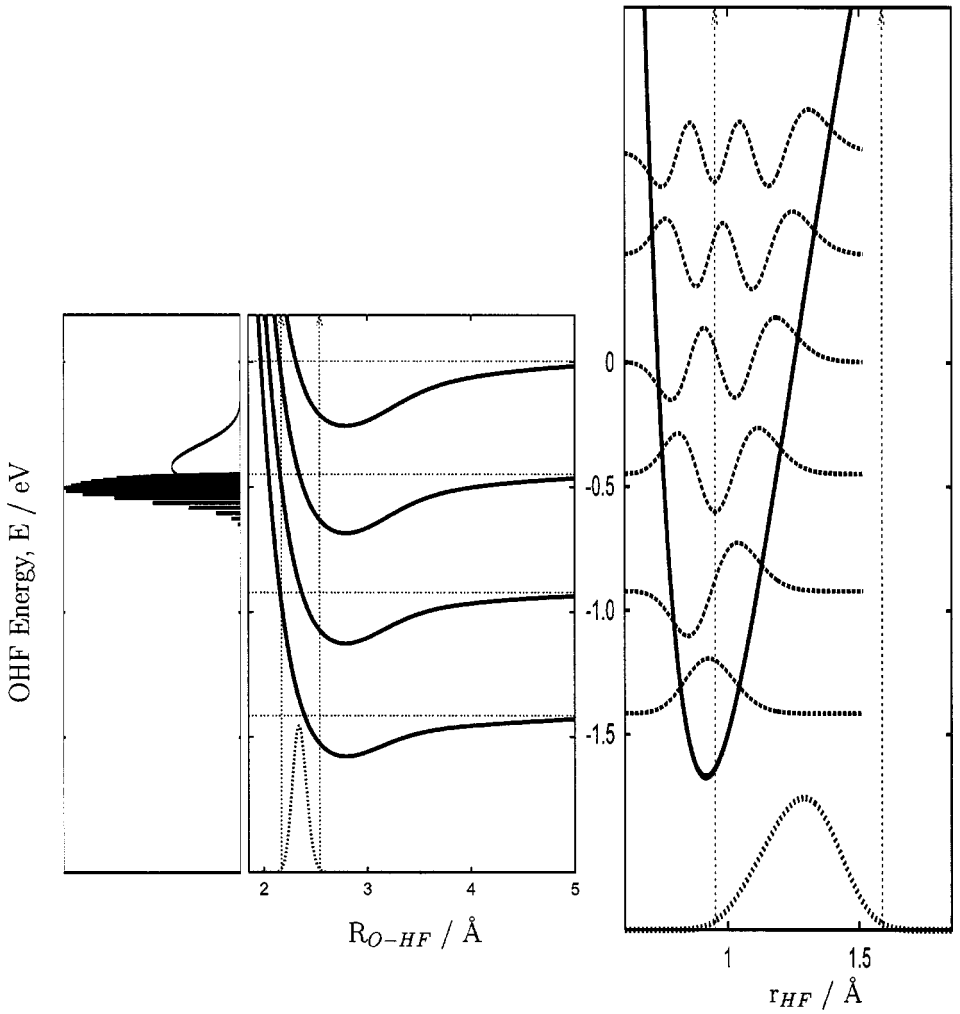

FIG. 8. Right panel, vibrational wave functions, φ_v, of bare HF placed at the corresponding eigenvalue on the HF PES. Middle panel, vibrationally average potentials, $\langle \varphi_v | V(R,r,\gamma=0) | \varphi_v \rangle$, for different HF vibrational levels as a function of R. In the lower part of these two panels the wave function amplitude of the OHF^- ground vibrational state is also plotted. Finally, at the left panel, the overlap between the initial vibrational OHF^- state and the final wave functions is shown for the case of $v=2$.

+F channel. However, the wave packet calculations can properly describe this new rearrangement channel, and the resonances become much broader so that it is possible to converge the time integration. Above zero, the total flux towards reactants and products is in very good agreement with the total absorption spectrum obtained from the autocorrelation function, better than 99%. The difference between these two calculations above zero can be taken as a way to visualize the role of the opening of the new rearrangement channel. The TICC results present the same progression of vibrational bands, as a continuation of those discussed for energies below zero. The wave packet results, however, show a gradual decrease of the absorption probability because above $v=3$ the outer turning point of the HF potential curve, in Fig. 8, disappears because of the opening of the new arrangement channel (see Fig. 7).

The combination of these two kinds of calculations allows us to study the evolution of the resonance lifetimes with energy, shown in Fig. 11. As expected, the lifetimes decrease with energy, because the anharmonicity makes that the vibrational channels become closer and the kinetic energy for dissociation reduces, as explained by the energy gap law.[48] For the lower resonances, the lifetime follows an exponential law with energy. However, near the OH+F dissociation threshold, the lifetimes are significantly shorter and do not follow such law anymore. The situation becomes more complex because some IVR with the OH vibration begins to play an important role.[45] Such sharp change in the evolution of the lifetimes with energy can also be viewed as originated by the opening of a new rearrangment channel.

D. Resonances above the OH+F threshold

Above this second threshold a new fragmentation pathway opens, leading to OH products, and the widths of resonances increase, as can be seen in Fig. 11. The frequencies of OH and HF vibrations become similar so that IVR between them become important. These resonances are located in the vicinity of the transition state and play an important role in the reaction dynamics.[20] It can be observed that these resonances cluster in small groups, or polyads, which are separated by ≈40 meV.

In Fig. 12 the spectrum for energies above this threshold and the final HF probability are compared with the reaction probability obtained for the $F+OH(v=0,j=0)$ collision at $J=0$ in paper I.[20] The two reaction probabilities are very different thus showing the strong influence of the initial conditions. However, it is interesting to note that at the energies of the resonances appearing in the spectrum there is a sudden change in the reaction probabilities of the two processes. At

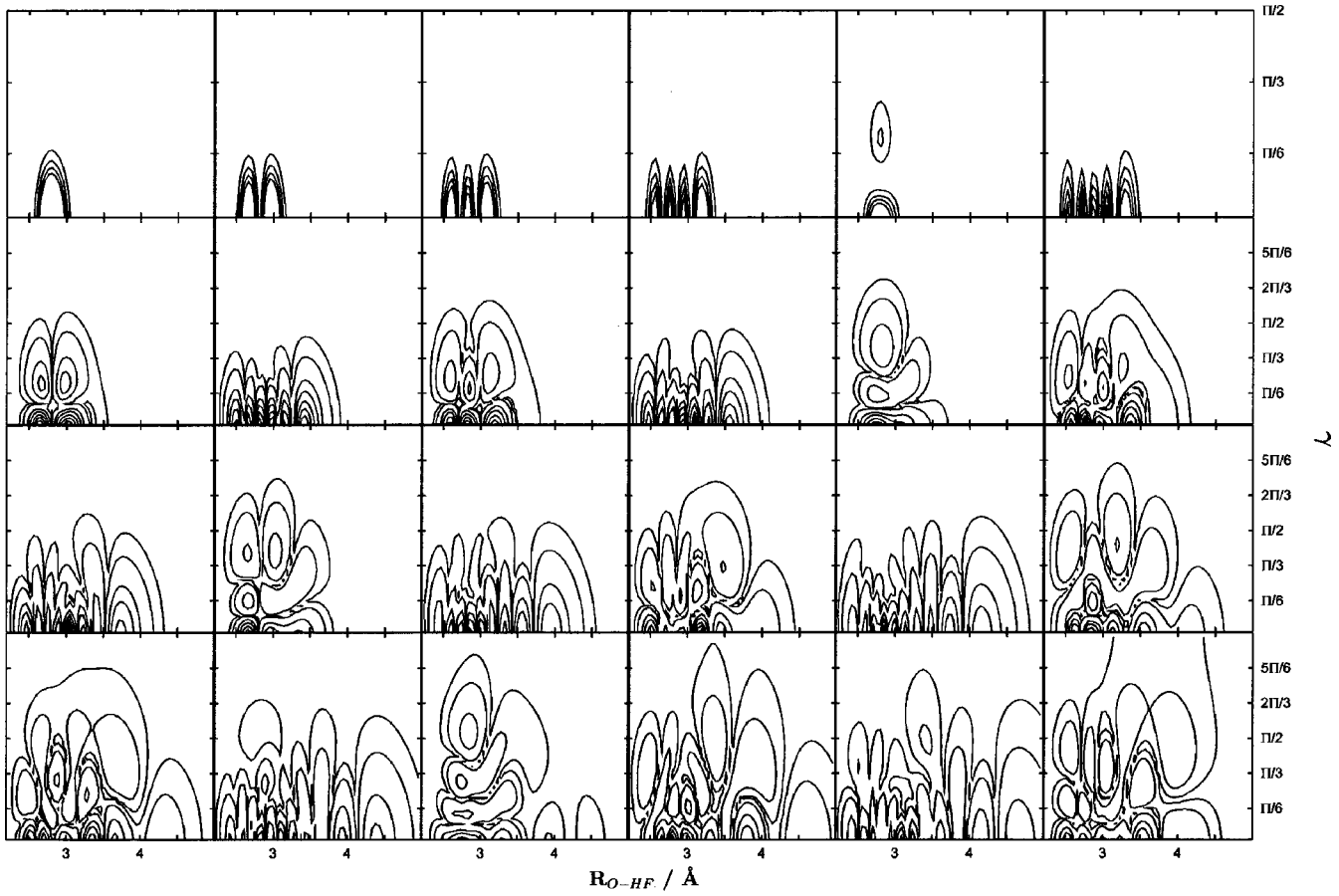

FIG. 9. Contour plots of the amplitude density of the quasibound states, for r frozen at the HF equilibrium distance, obtained for O–HF($v=1$).

this regard, two energy intervals can be considered. In the collision, there is a sort of dynamical zero-point energy, of $\approx$0.125 eV attributed to the bending motion as discussed in paper I. Below this energy, the reaction probability presents a clear resonant structure, which also appears in the photodetachment spectrum. About 0.125 eV, however, the collisional reaction probability increases up to 0.8 and hereafter decreases nearly monotonically with energy as a consequence of a direct reaction for a very exothermic reaction. However, this collisional reaction probability shows small structures for these higher energies which clearly appear in the photodetachment spectrum. Such structures are nearly unnoticeable in the collision, and for the reaction cross sections disappear completely as a consequence of the partial wave

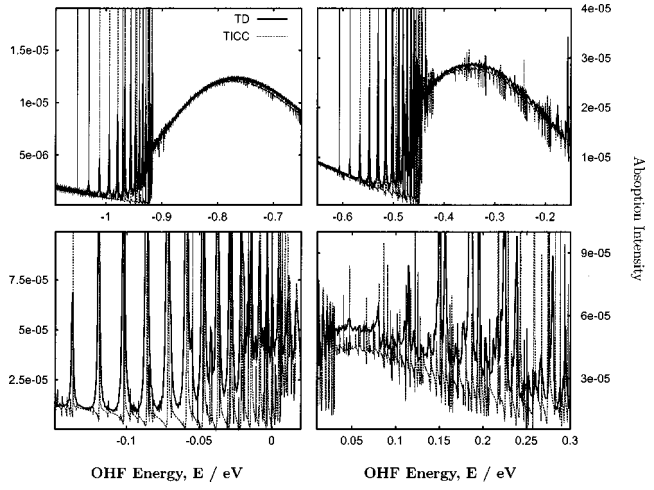

FIG. 10. Comparison of the spectra calculated with wave packets and a time-independent close-coupling method, with a limited vibrational basis set. The panels approximately correspond to the energy region of each vibrational band.

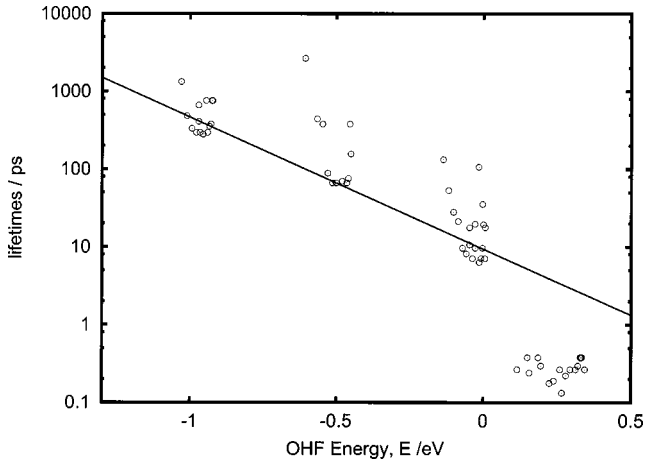

FIG. 11. Resonance lifetimes (in ps) as a function of energy (in eV), as obtained by doing individual fits to a Lorentzian function in the vicinity of the rather well isolated resonances of the spectrum calculated with the TICC in rather fine energy grid.

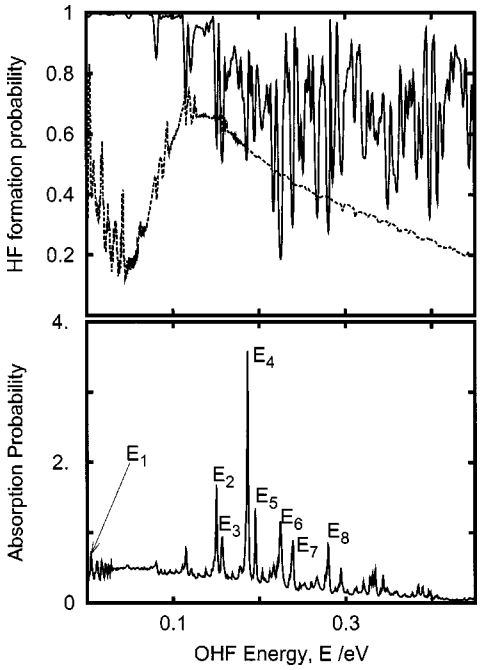

FIG. 12. Spectrum (bottom panel) and final OH probabilities (top panel) obtained in the photodetachment process (full line) compared to that obtained in the F+OH($v=0,j=0$) collision (dashed line) for zero total angular momentum in paper I.

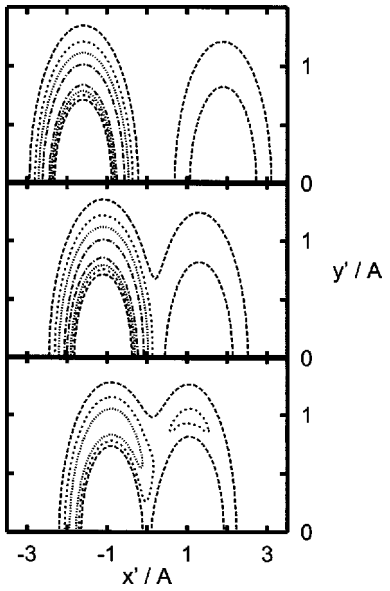

FIG. 13. Contour plots of the OHF($^3A''$) PES as a function of $x' = R_{\mathrm{H-OF}} \cos \gamma'$ and $y' = R_{\mathrm{H-OF}} \sin \gamma'$, in Å, for three different OF distances. Bottom panel, $r_{\mathrm{OF}} = 1.965$ Å, corresponding to the saddle point. Middle panel, $r_{\mathrm{OF}} = 2.4$ Å the equilibrium distance in the OHF^- precursor. Top panel, $r_{\mathrm{OF}} = 3.5$ Å closer to dissociation. The contours are -1.2, -0.5, 0, and 1 eV, with respect to the F+OH($v=0$) threshold.

averaging. However, its effect on other less averaged quantities, such as state-to-state differential cross section, could remain larger. Similarly, in the analogous $O(^3P)+HCl$ reaction the resonances appearing in the cumulative reaction probabilities were attributed to the two van der Waals minima in the entrance and exit channels.[14] Moreover, these resonances appear in classical simulations of the OH+F collisions[20] clearly demonstrating the existence of periodic orbits on the top of the saddle point. Since below the dynamical threshold these resonances mediate the reaction the spectroscopic determination of such structures may be of great interest.

These HLH' resonances correspond to the light hydrogen atom vibrating between the two heavier fluorine and oxygen atoms,[23] which may be considered to remain motionless. This suggests a natural adiabatic separation between the fast hydrogen atom and the slow heavier atoms, as suggested by Kubach and co-workers,[49,50] similar to the Born–Oppenheimer approximation. The natural coordinates to perform such approximation are a new set of Jacobi coordinates: the FO internuclear vector, $\mathbf{r}_{\mathrm{OF}}$, and the vector joining the FO center-of-mass to the H atom, $\mathbf{R}_{\mathrm{H-OF}}$, γ' being the angle between them. The PES in these new coordinates for frozen r_{OF} distances are shown in Fig. 13. At large r_{OF} distances, there is nearly a free rotation–vibration motion of the H atom around the F or O atoms. As long as the heavier atoms approach each other, the H atom can ''pass'' from F to O and vice versa. The resonance between the HF and OH vibrations stabilize the system at the precise energies where nearly quasibound states appear, in a clear analogy to what happens in H_2^+.[49,50] Instead of calculating the motion of H atom for each r_{OF} distance, as performed by Kubach and co-workers,[9,49,50] we analyze such resonances using the 3D wave packet calculations discussed above.

The quasibound components, ϕ_k^0 of the wave packets near the resonances are obtained by[38]

$$\phi_k^0(\mathbf{r},\mathbf{R}) \approx \int_0^\infty dt\, e^{-i(E_k - i\Gamma_k)^* t/\hbar}\ \Psi(\mathbf{r},\mathbf{R},t), \tag{10}$$

where E_k are the energies of the resonances, and Γ_k their widths (here we used $\Gamma_k = 5\ \mathrm{cm}^{-1}$). Once the integration in time is finished, these approximated quasibound functions are transformed to the new $\mathbf{r}_{\mathrm{OF}}$ and $\mathbf{R}_{\mathrm{H-OF}}$ coordinates. Contour plots of the probability density of some of the resonances are shown in Fig. 14. The three different panels correspond to $r_{\mathrm{OF}} = 1.89$ (the sum of the HF and OH equilibrium distances), 2.4 (the equilibrium distance of the parent OHF^-), and 3.5 Å (near dissociation), and the corresponding energy allows to identify each resonance.

At long r_{OF} distances, the H atom can rotate and vibrate nearly freely around each of the two heavier atoms. This situation allows a clear assignment of the resonances. Nearly all resonances correspond to $v_{\mathrm{HF}} = 3$ and $v_{\mathrm{OH}} = 0$, what is not surprising looking at the energy diagram in Fig. 7. At $r_{\mathrm{OF}} = 3.4$ Å it is still possible to identify rotational quantum numbers associated to either HF or OH. In fact the resonances can be distinguished by the rotational quantum numbers associated to each diatomic. It is also notorious that for nearly all the resonances chosen, the most significant in the spectrum, the rotational quantum number associated to HF and OH are nearly the same. This fact is probably due to the energy similarity of OH($v=0$) and HF($v=3$) thresholds, and that their rotational constants are very similar. Also, the amplitude of these resonances at the saddle point, for $r_{\mathrm{OF}} = 1.965$ Å, is rather significant, thus providing information

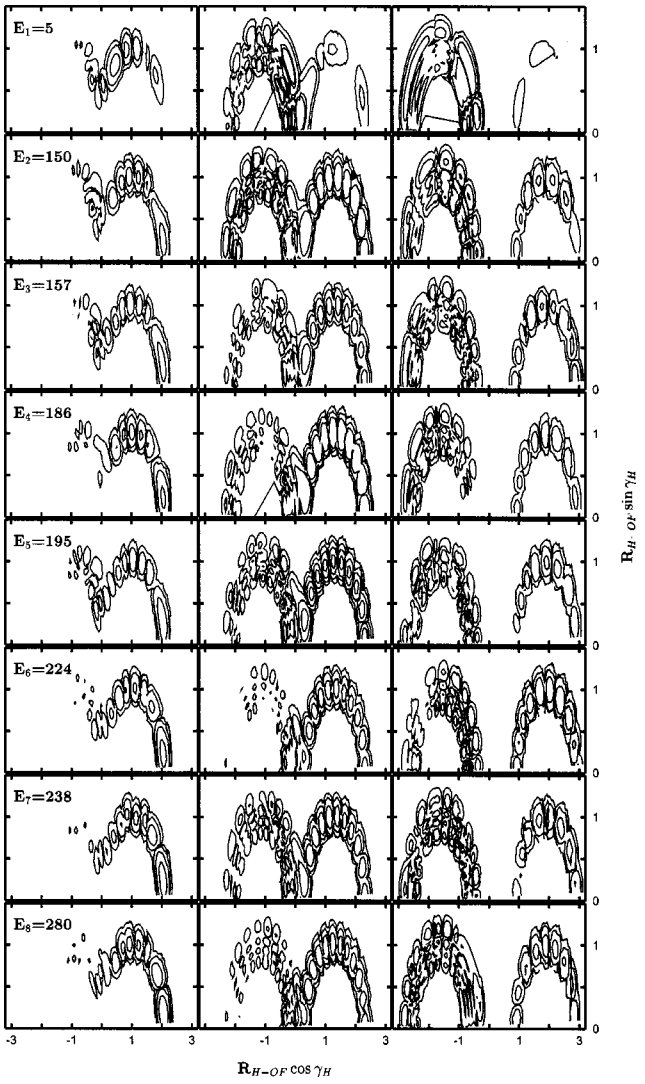

FIG. 14. Contour plots of the density probability of several HLH resonances. The energy of the resonances are in meV, distances are in Å, and three contours are chosen with an order of magnitude of density probability difference, to distinguish the wave functions structures. Left panels for $r_{OF}=1.965$ Å, middle panels for $r_{OF}=2.4$ Å, and right panels for $r_{OF}=3.5$ Å.

about the transition state region. Other combinations of quantum numbers could produce less stable orbits leading to broader resonances nearly undistinguishible from the background of the spectrum.

As r_{OF} becomes shorter, the densities associated to each diatomic overlap and the bending motion becomes more and more constrained, essentially towards the OH. If the distribution at short distances would place on the HF region, the system will fragmentate rapidly because the potential becomes pretty much repulsive, see Fig. 7. This last situation would yield less stable orbits associated to broader resonances.

IV. CONCLUSIONS

In this work a detailed three-dimensional study of the OHF^- photodetachment spectrum has been performed. The ground $OHF^-(^2A')$ PES has been calculated and fitted in three dimensions. The first excited $^2A''$ state, degenerate to the ground state at collinear geometry, has been estimated to have a larger bending frequency, thus not contributing significantly at the low temperatures of the experimental conditions.

The photodetachment spectrum towards $OHF(^3A'')$ has been calculated with a wave packet method using a three-dimensional PES recently obtained.[20] The spectrum agrees pretty well with the experimental sequence of broad bands.[21] In the simulated spectrum, the spectrum consists of a sequence of bands, each one formed by a broad continuous absorption component and a set of narrow resonances, which may be washed out in the experiment by the rotational average and the lower energy resolution. The bands are associated to the HF vibrational levels and the resonances at low energies to the well in the O+HF channel. These resonances did not appear in previous simulations of the spectrum obtained in two-dimensional collinear models.[21,22]

Above the OH+F dissociation threshold, however, the continuous bands seems to disappear and only a sequence of broader resonances survive. These resonances are attributed to HLH' type resonances and coincide with some structures obtained in the reaction probabilities for the $OH(v,j)+F$ collisions.[20] These resonances determine important features of the reaction dynamics. As an example in the collisions at energies below the kinematic threshold, at ≈ 0.125 eV, the reaction only takes place at these resonances, clearly demonstrating that they mediate the reaction. These resonances have been analyzed using the bound components obtained through a pseudospectral method applied to the wave packet. With this study, the structure of the resonances is understood and perfectly assigned. It would be therefore important to obtain a better resolved spectroscopic characterization of these HLH' resonances to get a more detailed information of the transition state region. Moreover, in the $OH(^2\Pi)+F(^2P)$ reactive collisions these resonances should have an important effect on different properties, such as final vibrational states of products and differential cross sections.

The two bands, labeled E and F, appearing at lower electron kinetic energies in the experimental spectrum appear in a region where there are many resonances in the present simulation. However, it is unlikely, that these resonances are responsible for those peaks. It is more probable that they are originated by other excited states.

The other two triplet states correlating to the same asymptotes, one $^3A'$ and $^3A''$, have essentially the same energetics. The associated spectra are expected to show the same progression of vibrational bands. Some shifts on the bands are expected because these triplets do not have as deep wells. The average over triplets would wash out the minima appearing at present, approaching to the shoulderlike structure of the experimental results. In addition, these two triplets states are also expected to contribute at the low electron kinetic energies were the experimental peaks E and F appear.

The singlet states connecting the $OH(^2\Pi)+F(^2P)$ to the $HF(^1\Sigma)+O(^1D)$ asymptotes have higher energies, and would contribute at the lower electron kinetic energies. The analysis of the contribution of all these excited electronic states, singlets and and triplets, is now in progress.[42]

ACKNOWLEDGMENTS

This work has been supported by MCYT(Spain), under Grant Nos. BFM2001-2179, BQU2001-0152, and BQU2002-04462-C02-01.

[1] R. P. Wayne, *Chemistry of Atmospheres* (Oxford University Press, Oxford, 2000).
[2] A. R. Ravishankara, G. Smith, R. T. Watson, and D. D. Davis, J. Phys. Chem. **81**, 2220 (1977).
[3] R. G. Macdonald and C. B. Moore, J. Chem. Phys. **68**, 513 (1978).
[4] D. J. Rakestraw, K. G. McKendrick, and R. N. Zare, J. Chem. Phys. **87**, 7341 (1987).
[5] K. Mahmud, J-S. Kim, and A. Fontijn, J. Phys. Chem. **94**, 2994 (1990).
[6] R. Zhang, W. J. van der Zande, M. J. Bronikowski, and R. N. Zare, J. Chem. Phys. **94**, 2704 (1991).
[7] M. J. Davis, H. Koizumi, G. C. Schatz, S. E. Bradforth, and D. M. Neumark, J. Chem. Phys. **101**, 4708 (1994).
[8] H. Koizumi, G. C. Schatz, and M. S. Gordon, J. Chem. Phys. **95**, 6421 (1991).
[9] N. Rougeau and C. Kubach, Chem. Phys. Lett. **274**, 535 (1997).
[10] B. Ramachandran, E. A. Schrader III, J. Senekowitsch, and R. E. Wyatt, J. Chem. Phys. **111**, 3862 (1999).
[11] L. Wang, C. Kalyanaraman, and A. B. McCoy, J. Chem. Phys. **110**, 11221 (1999).
[12] F. J. Aoiz, L. Bañares, J. F. Castillo, M. Menéndez, and J. E. Verdasco, Phys. Chem. Chem. Phys. **1**, 1149 (1999).
[13] K. Nobusada, H. Nakamura, Y. Lin, and B. Ramachandran, J. Chem. Phys. **113**, 1018 (2000).
[14] T. Xie, D. Wang, J. M. Bowman, and D. E. Manolopoulos, J. Chem. Phys. **116**, 7461 (2002).
[15] T. Xie, J. M. Bowman, K. A. Peterson, and B. Ramachandran, J. Chem. Phys. **119**, 9601 (2003).
[16] B. Ramachandran and K. A. Peterson, J. Chem. Phys. **119**, 9590 (2003).
[17] C. D. Walter and H. G. Wagner, Ber. Bunsenges. Phys. Chem. **87**, 403 (1983).
[18] J. J. Sloan, D. G. Watson, J. M. Williamson, and S. Wright, J. Chem. Phys. **75**, 1190 (1981).
[19] S. Gómez-Carrasco, L. González-Sánchez, A. Aguado, M. Paniagua, O. Roncero, M. L. Hernández, and J. M. Alvariño, Chem. Phys. Lett. **383**, 35 (2004).
[20] S. Gómez-Carrasco, L. González-Sánchez, A. Aguado, M. Paniagua, O. Roncero, M. L. Hernández, and J. M. Alvariño (unpublished).
[21] S. E. Bradforth, D. W. Arnold, R. B. Metz, A. Weaver, and D. M. Neumark, J. Phys. Chem. **95**, 8066 (1991).
[22] R. N. Dixon and H. Tachikawa, Mol. Phys. **97**, 195 (1999).
[23] R. B. Metz, S. E. Bradforth, and D. M. Neumark, Adv. Chem. Phys. **81**, 1 (1992).
[24] D. M. Neumark, Annu. Rev. Phys. Chem. **43**, 153 (1992).
[25] A. Weaver, R. B. Metz, S. E. Bradforth, and D. M. Neumark, J. Phys. Chem. **92**, 5558 (1988).
[26] J. M. Bowman and B. Gazdy, J. Phys. Chem. **93**, 5129 (1989).
[27] T. H. Dunning, Jr., J. Chem. Phys. **90**, 1007 (1989).
[28] R. A. Kendall, T. H. Dunning, Jr., and R. J. Harrison, J. Chem. Phys. **96**, 6796 (1992).
[29] H.-J. Werner and P. J. Knowles, J. Chem. Phys. **82**, 5053 (1985).
[30] H.-J. Werner and P. J. Knowles, J. Chem. Phys. **89**, 5803 (1988).
[31] H.-J. Werner and P. J. Knowles, Chem. Phys. Lett. **145**, 514 (1988).
[32] E. R. Davidson, J. Comput. Phys. **17**, 87 (1975).
[33] MOLPRO is a package of *ab initio* programs designed by H.-J. Werner and P. J. Knowles, with contributions from J. Almlöf, R. D. Amos, A. Berning, *et al.* (version 2002.7).
[34] A. Aguado and M. Paniagua, J. Chem. Phys. **96**, 1265 (1992).
[35] R. N. Zare, *Angular Momentum* (Wiley, New York, 1988).
[36] A. Aguado, M. Lara, M. Paniagua, and O. Roncero, J. Chem. Phys. **114**, 3440 (2001).
[37] G. C. Schatz, J. Phys. Chem. **94**, 6157 (1990).
[38] M. Paniagua, A. Aguado, M. Lara, and O. Roncero, J. Chem. Phys. **111**, 6712 (1999).
[39] A. Aguado, M. Paniagua, C. Sanz, and O. Roncero, J. Chem. Phys. **119**, 10088 (2003).
[40] H. Tal-Ezer and R. Kosloff, J. Chem. Phys. **81**, 3967 (1984).
[41] C. Leforestier, R. H. Bisseling, C. Cerjan, *et al.*, J. Comput. Phys. **94**, 59 (1991).
[42] L. González-Sánchez, S. Gómez-Carrasco, A. Aguado, M. Paniagua, M. L. Hernández, J. M. Alvariño, and O. Roncero (unpublished).
[43] O. Roncero, J. Campos-Martínez, M. I. Hernández, G. Delgado-Barrio, P. Villarreal, and J. Rubayo-Soneira, J. Chem. Phys. **115**, 2566 (2001).
[44] G. G. Balint-Kurti, R. N. Dixon, and C. C. Marston, J. Chem. Soc., Faraday Trans. **86**, 1741 (1990).
[45] O. Roncero, D. Caloto, K. C. Janda, and N. Halberstadt, J. Chem. Phys. **107**, 1406 (1997).
[46] O. Roncero, J. A. Beswick, N. Halberstadt, P. Villarreal, and G. Delgado-Barrio, J. Chem. Phys. **92**, 3348 (1990).
[47] F. X. Gadéa, H. Berriche, O. Roncero, P. Villarreal, and G. Delgado-Barrio, J. Chem. Phys. **107**, 10515 (1997).
[48] J. A. Beswick and J. Jortner, Adv. Chem. Phys. **47**, 363 (1981).
[49] C. Kubach, G. Nguyen, and M. Richard-Viard, J. Chem. Phys. **94**, 1929 (1991).
[50] N. Rougeau, S. Marcotte, and C. Kubach, J. Chem. Phys. **105**, 8653 (1996).